IEEE Access
Multidisciplinary | Rapid Review | Open Access Journal

SPECIAL SECTION ON EVOLVING TECHNOLOGIES IN ENERGY STORAGE SYSTEMS FOR ENERGY SYSTEMS APPLICATIONS

Received January 28, 2021, accepted February 9, 2021, date of publication February 16, 2021, date of current version February 26, 2021.

Digital Object Identifier 10.1109/ACCESS.2021.3059718

Optimization Method and Reduced-Order Steady-State Model for Variable-Speed Pump-Turbine Unit

WEIWEI YAO[1], (Member, IEEE), CHANGHONG DENG[1], (Member, IEEE), AND PENG PENG[2]
[1]School of Electrical Engineering and Automation, Wuhan University, Wuhan 430072, China
[2]China Southern Power Grid Power Generation Company, Guangzhou 510630, China

Corresponding author: Changhong Deng (dengch@whu.edu.cn)

This work was supported in part by the National Key Research and Development Program of China under Grant 2017YFB0903700.

ABSTRACT Increased attention has been paid to the high-capacity variable-speed pumped storage to stabilize the large-scale renewable energy. Nevertheless, the optimum reference values of variable-speed units (i.e., the optimum speed and optimum gate opening) come from the actual operating data from power plants or the model pump-turbine test from manufacturers. It is generally a commercial secret, and no historical data is available for a new power plant. For general researchers, it is not easy to obtain relevant data. Therefore, this paper proposes an optimization method for the variable-speed unit and establishes a simplified steady-state model that can be used for medium and long-term power system research. First, based on the pump-turbine's performance curves, this paper presents an optimization method for the variable-speed unit in turbine and pump mode without additional tests, aiming to optimize the turbine's efficiency and track the input power of the pump. Second, the concept of ''steady operation area in non-optimum condition'' is proposed based on the non-linear characteristics of the optimum operating condition curve. Finally, simplified steady-state models of the variable-speed unit are established, and the model validation has been tested in typical scenario analysis. The results show that the variable-speed unit's steady-state operating characteristic can be described by this simplified linear model, based on the power, the head, and the optimum speed (or the gate opening). This simplified model's percentage error is less than 5%, which meets engineering accuracy requirements. The error mainly comes from the linear correlation coefficient of the optimum operating condition curve and the operating head's deviation from the design head. This model is available for power system planning and dispatch.

INDEX TERMS Variable-speed pumped storage, maximum efficiency points tracking, the steady operation area in non-optimum condition, optimum speed and opening, variable-speed operation ranges.

I. INTRODUCTION

Due to the challenges to the safe and stable operation of the power grid brought by the grid connection of large-scale renewable energy (i.e., the power fluctuation in the daytime, the frequency regulation in the nighttime), the energy storage system must be equipped for buffering [1], [2]. The variable-speed pumped storage technology with power electronics has become one of the most attractive options in the high-capacity energy storage areas (>100MW) [3]. It also has the advantages of the large capacity of the conventional pumped storage and the fast response rate of the electrochemical energy storage at the same time [4]. The variable-speed pumped storage unit has the following advantages [5], [6]: (1) the comprehensive operation efficiency of a power plant can be improved, especially during part-load operation; (2) the output range of the unit can be changed and active power regulation ability can be improved; (3) the unit can transiently respond to the power fluctuation of the power grid in milliseconds by flywheel effect, which significantly improved the frequency regulation performance.

At present, studies on the variable-speed pumped storage unit are mainly focused on the dynamic control of units [7], such as the frequency adjustment of the power grid in pump mode [8], [9], the rapid dynamic response analysis in the asynchronous condition [10], the joint optimization operation

The associate editor coordinating the review of this manuscript and approving it for publication was Sanjeevikumar Padmanaban.

with the large-scale renewable energy [11], [12], and the commercial benefit analysis of the variable-speed unit [13], [14]. Some studies also focus on the joint system's steady-state operation [15], [16]. Unfortunately, as the basis of studies, there remain some problems in the unit's steady-state model, which cannot reflect the variable-speed unit's characteristics under the premise of ensuring computational efficiency [17], [18]. For example, in the study of medium and long-term planning and scheduling, variable-speed units are often regarded as conventional fixed-speed units [19]. The operating efficiency does not vary with the operating conditions. It does not reflect the input power range's change under the various working conditions and the influence factors that cause this change in pump mode.

To establish a suitable steady-state model, we should analyze the operation mechanism of the variable-speed unit. In a joint system composed of large-scale renewable energy, the variable-speed pumped storage unit needs to respond to the power fluctuations in real-time and is also restricted by real-time changes because of the reservoir-heads curve. It will lead to continuous changes of optimal operating conditions, so the variable-speed unit must simultaneously change the speed and gate opening to achieve real-time tracking of optimal working conditions. The steady-state modeling process of the variable-speed unit is the refinement of the optimization of the operating conditions. Moreover, the optimization results (such as the optimum gate opening, the optimum speed, and the highest efficiency) will also become the dynamic control system's input, as the unit control system's optimum reference value. At present, this optimum reference value mainly comes from the power plant's actual operation data or the manufacturer's model test [20]–[23]. All the data is generally the commercial secret, and no historical data is available for a new power plant. Moreover, it should be noted that each mode's optimization goal is different during variable-speed operation: the goal is for maximizing efficiency in turbine mode, but for power tracking in pump mode.

In summary, we need first to analyze the variable-speed unit's optimization process in two modes and then establish a steady-state model. So far, some scholars have proposed some modeling methods for variable-speed turbines or pump-turbines. For example, [19] proposed an optimum efficiency model for a propeller-type turbine for variable-speed operation, but the model contains non-linear factors such as exponential and reciprocal terms. The complexity is too high, and it is not suitable for large-scale grid-level calculations. The propeller type turbine is not the first choice for prime movers of large-capacity (>100MW) pumped storage units because the gate opening cannot be adjusted. Reference [24] gives a bulb-type turbine's optimum efficiency model based on speed and flow rate. This model also contains absolute value terms and higher-order terms, which are more suitable for transient analysis in PSCAD/EMTDC. Besides, bulb-type turbines are generally only suitable for small-capacity and low-head applications, and their gate openings cannot be adjusted. The neural network is used to study the optimum operating conditions of axis-flow propeller turbine with variable-speed operation in [25]. The response is filled into the look-up table as the neural network's training set through the combination testes of different flow and gate opening. However, this method is highly non-linear and discontinuous and usually cannot meet large-scale calculations' speed requirements at the grid-level. Reference [26] also made the same attempt. Reference [27] uses the simplest polynomial fitting method to track the optimum operating conditions, but it ignores the influence of flow changes in different optimum operating conditions. Reference [28] proposed an optimum model based on Hill Chart, which can be used to study the variable-speed control. Most of the above models do not consider the power tracking function of variable-speed pumped storage units in pump mode.

This paper's remainder is organized as follows: In Section II, optimizing the speed and gate opening is deduced based on the necessary data (such as the Hill Chart and the performance curve) provided by the manufacturer. In Section III, the concept of ''steady operation area in non-optimum condition'' is proposed for the first time. The optimization methods and matters needing attention are explored when the speed reaches the minimum speed, and the optimum operating condition curve is non-monotonic. Finally, in Section IV, the variable-speed unit's steady-state simplified model is established in two modes, including the optimum speed and opening model. In Section V, we conduct the model validation and error analysis under the different scenarios. Section VI is the conclusion.

The present paper attempts to highlight:

1) An optimization method for variable-speed pumped storage units in two modes is proposed, especially considering the concept of ''steady operation area in non-optimum condition.''
2) A simplified steady-state model of the variable-speed unit is established based on characteristic curves of pump-turbine, which is suitable for large-scale calculations

II. OPTIMIZATION METHODS FOR THE VARIABLE-SPEED PUMP-TURBINE IN DIFFERENT MODES

As mentioned above, analyzing the optimization process of variable-speed operation is the basis of establishing a simplified steady-state model. Because of the different purposes in the two modes, the optimization methods are proposed in this section.

The time scale corresponding to the steady-state operation is mainly related to the prime mover but has nothing to do with the millisecond-level fast dynamic response; that is, the electronic converter's transient process does not need to be considered. There is little difference in the pump-turbines used in the variable-speed unit and traditional fixed-speed unit. Large commercial variable-speed units mainly adopt Francis turbine [19], [29], [30], and a few also adopt Deriaz turbine since the benefit of the pumped storage plants significantly increases with the increase of the head [31].

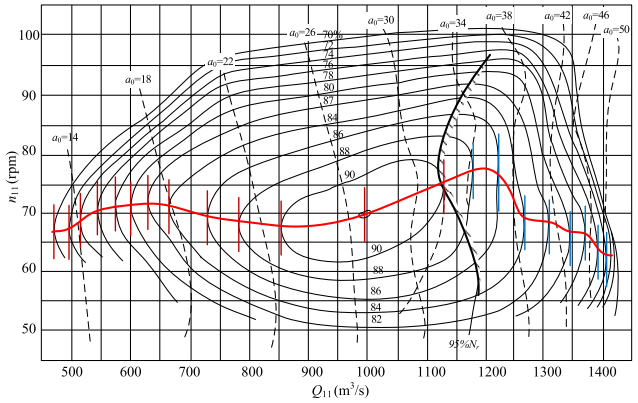

FIGURE 1. Hill Chart of a model Francis turbine [45].

The pump-turbine is hydraulically designed according to the pump mode and verified according to the turbine mode. The unit often deviates from the optimum operating condition [26], [32]. After the adoption of the variable-speed technology, the pump-turbine has an additional degree of freedom. The gate opening and speed can be controlled simultaneously so that optimum efficiency can be tracked within a broader range [33]. The operation range of the unit can be significantly expanded in pump mode [34]. The following is an analysis of these two modes.

A. EFFICIENCY OPTIMIZATION METHOD IN TURBINE MODE

The Hill Chart of a model turbine (Fig. 1) is the most basic data provided by the equipment manufacturer during the acceptance procedure [35]. According to the IEC-60193 standard, the Hill Chart of models is expressed by unit values, the unit speed n_{11}, the unit flow Q_{11}, and the unit power P_{11}, based on the similarity law [36]. Mathematically,

$$\frac{nD}{\sqrt{H}} = const1 = n_{11} \tag{1}$$

$$\frac{Q}{D^2\sqrt{H}} = const2 = Q_{11} \tag{2}$$

$$\frac{P}{D^2 H\sqrt{H}} = const3 = P_{11} \tag{3}$$

where n is the mechanical speed, H is the head, Q is the flow, and D is the runner diameter.

When the unit flow Q_{11} is constant, η will vary with n_{11}, marked as curve $C1$ of efficiency η (see Fig. 1). It can be written as

$$C1 : \eta = f_1(n_{11})|_{Q_{11}} \tag{4}$$

$C1$ is a family of curves. Each curve in $C1$ has a maximum efficiency $\eta_{\max}$, or each Q_{11} uniquely corresponds to an optimum operating point, due to the existence of an iso-efficiency circle. The optimum operating condition curve (the red curve in Fig. 1) of the turbine is obtained by connecting all the optimum operating points. Each $Q_{11.\text{opt}}$ also corresponds to the maximum efficiency $\eta_{\max}$ and the optimum unit speed $n_{11.\text{opt}}$, marked as the curve $C2$ and the curve $C3$.

$$C2 : \eta_{max} = f_2(Q_{11.opt}) \tag{5}$$

$$C3 : n_{11.opt} = f_3(Q_{11.opt}) \tag{6}$$

The energy conversion equation can be written as

$$P_e = P\eta_e \tag{7}$$

$$P = 9.81HQ\eta \tag{8}$$

where P_e is the output power of the motor-generator, P is the output power of the pump-turbine, H is the head, Q is the flow, η_e is the motor-generator efficiency, and η is the turbine-turbine efficiency in turbine mode.

After substituting (2) and (8) into (3), we can obtain

$$P_{11} = 9.81Q_{11}\eta \tag{9}$$

Based on the maximum efficiency curve $C2$ and (9), we can obtain the curve $C4$ of the maximum unit output $P_{11.\max}$ in optimum operating condition.

$$C4 : P_{11.max} = 9.81Q_{11.opt}\eta_{max} = f_4(Q_{11.opt}) \tag{10}$$

Besides, we can also find the optimum guide vane opening $a_{0.\text{opt}}$ from the Hill Chart according to the optimum operating point, which is marked as curve $C5$.

$$C5 : a_{0.opt} = f_5\left(Q_{11.opt}\right)|_{n_{11.opt}} \tag{11}$$

To sum up, we can obtain the optimum speed n_{opt}, the optimum flow Q_{opt} and the gate opening $a_{0.\text{opt}}$ according to the head H and the output requirement P_e at the unit level. Moreover, these parameters can be further used as the basis of parameter adjustment of the excitation and speed control system. In the actual adjustment, the guide vane opening is used for coarse adjustment of load and speed, and the AC-excitation system is used for fine adjustment.

At the power station level, the efficiency changes in real-time with the change of head and load power and is finally fed back to the change of stored energy of the reservoir.

B. POWER OPTIMIZATION METHOD IN PUMP MODE

Unlike that in turbine mode, the variable-speed unit's most significant advantage in pump mode is to solve the problem that the input power cannot be changed during the fixed-speed operating, rather than to gain efficiency. Also, the power optimization in pump mode is still based on the Hill Chart (x-coordinate is n_{11}, y-coordinate is Q_{11}). Regrettably, it is not easy to obtain Hill Chart in the pump mode since the $H \sim Q$ and $n \sim Q$ curves change little with gate opening, and the iso-opening curve in the small flow area also intersects. Therefore, it is hard to expand the efficiency circle with the iso-opening curve in the coordinates $n_{11} \sim Q_{11}$. The common practice in the industry is to describe the pump performance using the measured values of a model pump at rated speed, as shown in Fig. 2. In this paper, optimization is also carried out on this basis, without additional physical model tests.

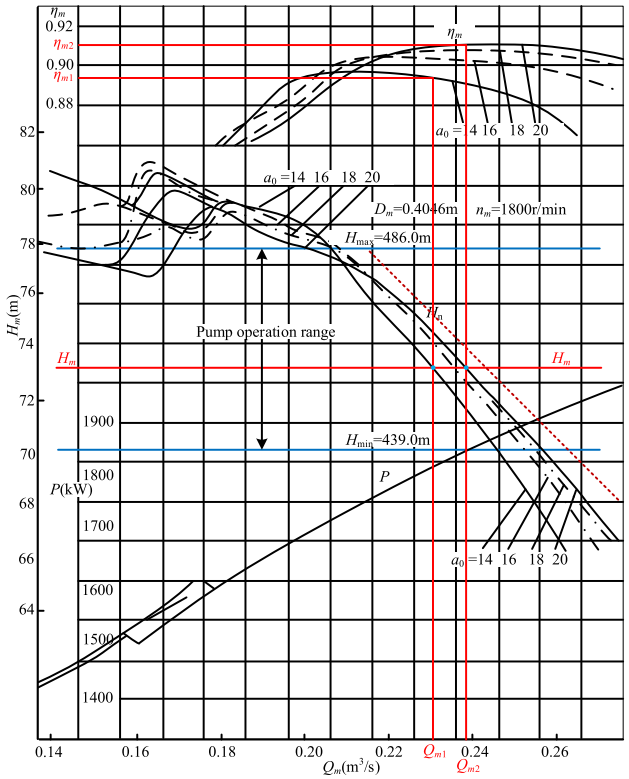

FIGURE 2. Performance characteristic of a model pump at rated speed.

When the speed changes little, the parabola of the similar operating points calculated according to pump affinity laws can be considered as the iso-efficiency curve. When a 556 kW pump's speed reaches 0.775 p.u., the error between the efficiency calculated according to the affinity laws and the actual value is no more than 0.12%. The error is even more minor for large pumps, according to [37]. The optimization process is as follows:

First, the head H_{m} of the model pump at rated speed is obtained based on the similarity law.

$$H_m = H\frac{D_m^2 n_m^2}{D^2 n^2} \tag{12}$$

where D and n are the diameter and rated speed of the prototype pump, respectively. D_{m} and n_{m} are the diameter and rated speed of the model pump, respectively.

Second, the flows ($Q_{\mathrm{m1}}, Q_{\mathrm{m2}}, \ldots$) under each opening ($a_{01}$, a_{02}, $\ldots$) at head H_{m} (the red horizontal line in Fig. 2) are found according to the family of curves $H \sim Q$ based on the model pump performance curves. Based on these flows, the efficiencies ($\eta_{\mathrm{m1}}, \eta_{\mathrm{m2}}, \ldots$) under the corresponding gate openings are found from the curves $\eta \sim Q$. After picking out the maximum one as the $\eta_{\max}$, the gate opening value $a_{0.\mathrm{opt}}$ and the flow value $Q_{\mathrm{m.opt}}$ are recorded, and this is the optimum operating point of the model pump under the current head H_{r}.

Third, the input power P_{m} of the model pump can be found in the curve $P \sim Q$ according to $Q_{\mathrm{m.opt}}$.

Then the actual power P (at rated speed) of the prototype pump is calculated as follows.

$$P = P_m\frac{n^3 D^5}{n_m^3 D_m^5} \tag{13}$$

Finally, the optimum speed n_{opt} of the prototype pump is calculated according to the real-time requirement P_{e}. Mathematically,

$$n_{opt} = n\sqrt[3]{\frac{P_e\eta_e}{P}} \tag{14}$$

The variable-speed unit's optimization flow chart in the two modes is shown in Fig. 3. A brief description is given below.

Firstly, at the power station level, the energy management system sets the sampling period (refresh rate) according to the dispatching time scale, initializes the head H(t), and calculates the speed limit range n_{lmt}. Then, the dispatching power command P_{e}(t) and mode transformation flag are received. The above parameters become the unit optimization module's input, which will perform optimization for different purposes according to different operating conditions. The purpose in turbine mode is efficiency optimization, and the purpose in pump mode is power tracking. The specific optimization process of the unit optimization module is shown in Section II. The output of the module is the optimal parameters of the current operating condition, including optimum speed n_{opt}(t), gate opening $a_{0.\mathrm{opt}}$(t), flow Q_{opt}(t), and maximum efficiency $\eta_{\max}$(t). These optimal parameters are used as the reference values (speed, opening, etc.) of the unit control system and the process parameters (efficiency, flow, etc.) of the energy management system. The energy management system calculates and updates the steady-state process at a specific refresh rate under necessary constraints such as head and reservoir capacity, cyclically.

III. ANALYSIS OF OPERATION CHARACTERISTICS OF VARIABLE-SPEED UNIT

We can quickly obtain the variable-speed unit's operation characteristic based on the optimization method in previous sections. The concept of "steady operation area in non-optimum condition" is proposed in this section as one of the steady-state simplified model analysis bases.

A. STEADY OPERATION AREA IN OPTIMUM CONDITION

Fig. 4 illustrates the optimal H~P operation curve of the turbine and pump mode. The solid black line area is the output range, and the red and blue dotted lines are the optimum speed and the optimum opening, respectively.

The H~P operation curve is divided into two areas. The orange background area is the unit's adjustable-speed operation range, where the unit can track the optimum efficiency in the turbine mode. The area is called "steady operation area in optimum condition" in this paper. When drawing the H~P operation curve, the optimum operating condition curve $Q_{11.\mathrm{opt}} \sim n_{11.\mathrm{opt}}$ is monotonically increasing by default. However, these curves of some types of runners are not

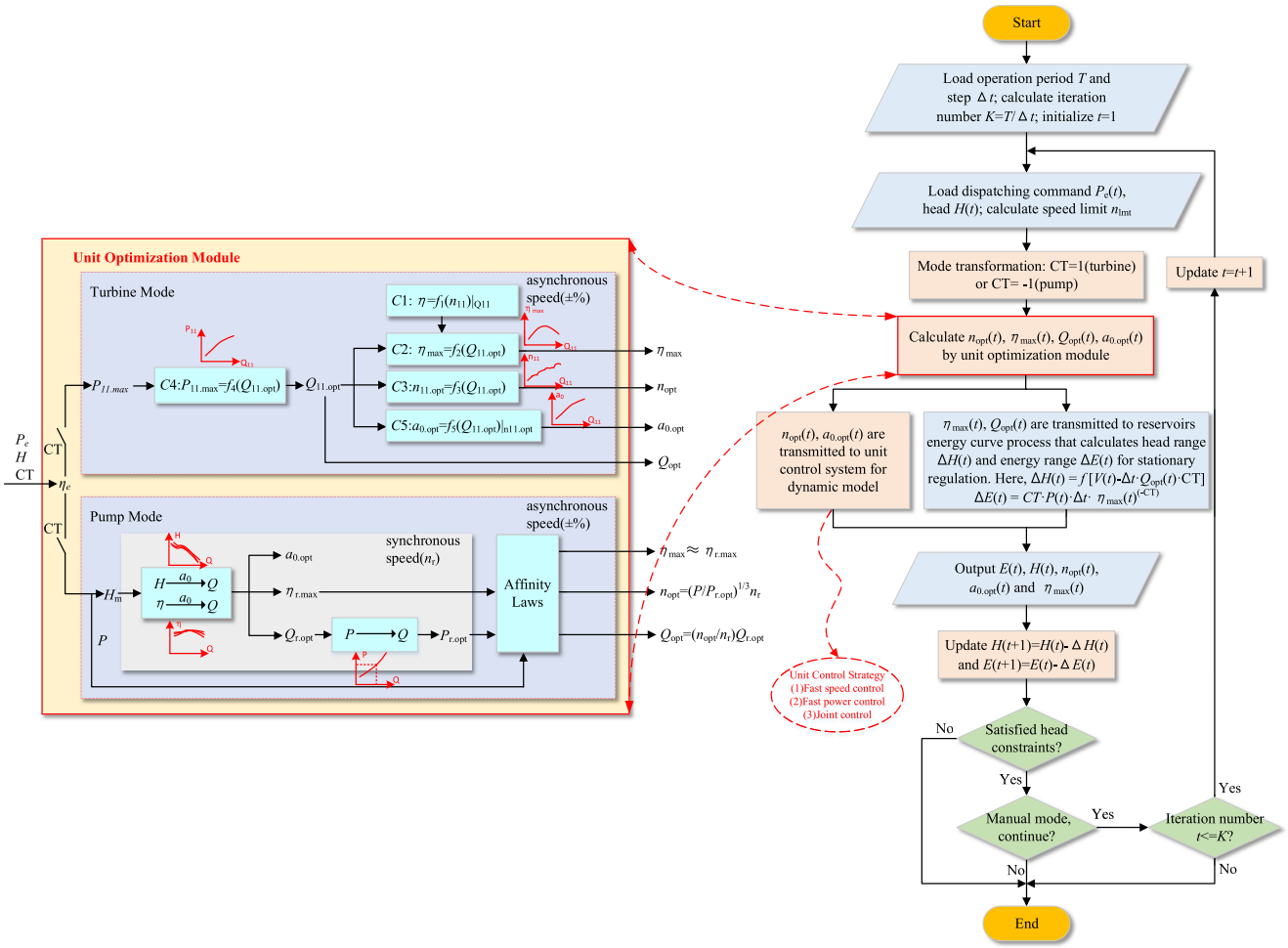

FIGURE 3. Optimization flow chart of a variable-speed unit in two modes.

monotonic completely (the red curve in Fig. 1). Therefore, the non-monotonic curves need to be analyzed.

According to the curve $C4$: $P_{11.\max} = 9.81 Q_{11.\text{opt}} \eta_{\max} = f4(Q_{11.\text{opt}})$, variable $\eta_{\max}$ changes within a small range (about 0.8∼0.95), and the changing amplitude of variable $Q_{11.\text{opt}}$ are more significant than that of variable $\eta_{\max}$. Therefore, the curve $C4$ must be a monotonically increasing function with $Q_{11.\text{opt}}$.

However, the curve $C3$: $n_{11.\text{opt}} = f3(Q_{11.\text{opt}})$, for some runners, does not have an inverse function. So the curve $C3$ may not be a continuous monotonic function.

So combining (3) and (10), when the head H is constant, we have

$$P_{max} = P_{11.max} D^2 H \sqrt{H} = k_1 f_4 \left(Q_{11.opt}\right)|_{\eta=\eta_{\max}} \tag{15}$$

Combining (1) and (6), when the head H is constant, we have

$$n_{opt} = n_{11.opt} \sqrt{H}/D = k_2 f_3 \left(Q_{11.opt}\right)|_{\eta=\eta_{\max}} \tag{16}$$

Therefore, considering $Q_{11.\text{opt}}$ as the intermediate variable, multiple $Q_{11.\text{opt}}$ may correspond to the same $n_{11.\text{opt}}$; that is, multiple $P_{\max}$ values correspond to the same n_{opt} in the H∼P operation curve. This phenomenon is noteworthy. In fact, these points represent completely different operating points, and they also correspond to different optimum opening values, respectively.

B. STEADY OPERATION AREA IN NON-OPTIMUM CONDITION

Another area with a blue background in the H∼P operation curve in Fig. 4(a) is called "steady operation area in non-optimum condition" in this paper. When the unit's optimum output power drops to a certain degree (near the 220MW-260MW in this case), the optimum speed also drops from the high speed to the minimum speed and cannot drop further. There is no speed control when the fixed-speed unit operates in the "steady operation area in the non-optimum condition." However, it is still possible for the variable-speed unit to achieve the optimum efficiency through speed control, so further analysis is necessary.

When H is constant, we have $P \propto P_{11}$ and $n \propto n_{11}$. As shown in Fig. 5, after the optimum speed n_{opt} drops to the minimum speed $n_{\min}$ along the optimum operating condition curve $C3$: $n_{11.\text{opt}} \sim Q_{11.\text{opt}}$, the speed cannot drop further, and the current operating point is the point A.

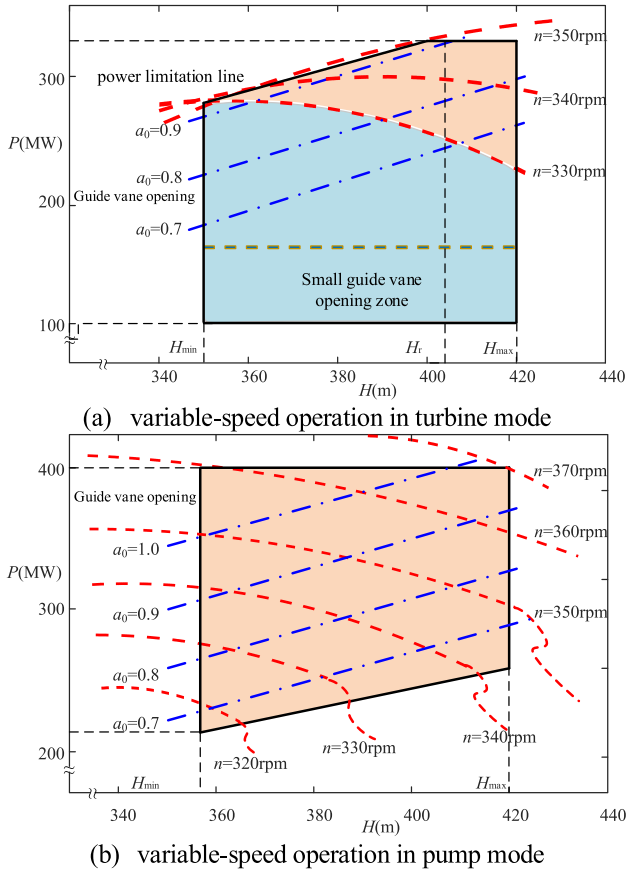

(a) variable-speed operation in turbine mode

(b) variable-speed operation in pump mode

FIGURE 4. Operation curve of the variable-speed unit: (a) turbine mode; (b) pump mode.

If further reduction of the power P is required, the maximum unit power $P_{11.\max} = 9.81 Q_{11.\mathrm{opt}} \eta_{\max}$ should continue to decrease. We assume that the curve $C3$ is monotonic (see Fig. 5(a)), so $n_{11.\mathrm{opt}}$ cannot decrease further, and $Q_{11.\mathrm{opt}}$ is unable to increase further. So the only path of point A is to enter the blue operation area. To always keep the maximum efficiency, point A moves left in a straight line perpendicularly to y-coordinate (path 1) instead of moving down along the curve $C3$, and the optimum speed of the unit in the ''steady operation area in non-optimum condition'' at this time is the minimum speed.

However, when the optimum operating condition curve $C3$ is non-monotonic (see Fig. 5(b)), point A continues to move left along the curve $C3$ (path 2) and enter the blue operation area to maximize the efficiency, and the optimization method at this time is the same as that in Section II. Finally, the optimum speed of the ''steady operation area in non-optimum condition'' will be greater than the minimum speed and change with external conditions in real-time.

All things considered, it is incorrect to state that the optimum speed is forever the minimum speed in the ''steady operation area in non-optimum condition'' (area with a blue background in Fig. 4(a). The emergence of this area is caused by the insufficient adjustment range, and this phenomenon is normal and essential. An exclusive emphasis on sufficient

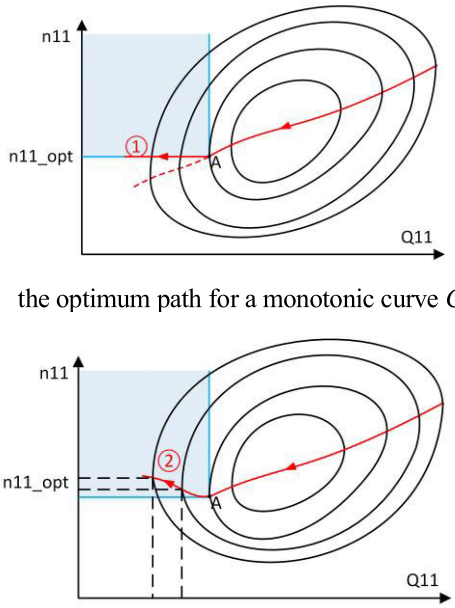

(a) the optimum path for a monotonic curve $C3$

(b) the optimum path for a non-monotonic curve $C3$

FIGURE 5. Optimum operation path when curve $C3$ is (a) monotonic or (b) non-monotonic.

adjustment range is insignificant and nonessential. The too high or too low speed will make the pump-turbine unstable and result in a sharp rise in the power converter costs.

IV. STEADY-STATE MODELING OF VARIABLE-SPEED UNIT AND ITS SIMPLIFICATION

Based on the analysis in the above sections, we have mastered the method and process of optimizing operating conditions in two modes and handling the treatment of the ''steady operation area in non-optimum condition.'' We will establish the simplified steady-state model for variable-speed operation and verify the scientificity and effectiveness in this section.

Fig. 6 illustrates the variable-speed unit's optimization results in two modes: optimum speed, optimum gate opening, and maximum efficiency. It is challenging to completely describe the variable-speed unit's steady-state operation characteristic by using a mathematical model. The pump-turbine flow-through part comprises components with different geometric shapes, and the internal water flow is very complicated. This section attempts to establish a simplified steady-state model, which can significantly reduce the large-scale computing consumption while meeting the research accuracy requirements.

A. VARIABLE-SPEED OPERATION RANGES

Uncontrolled expansion of the speed operation ranges is forbidden. The main reason is that it indicates a positive correlation between the operation range and the converter's capacity. The excessive operation ranges will result in a sharp rise in the costs of the power converter. Besides, the pump-turbine's stable operation zone is narrow than the fixed-speed turbine. The unstable phenomenon, such as cavitation and

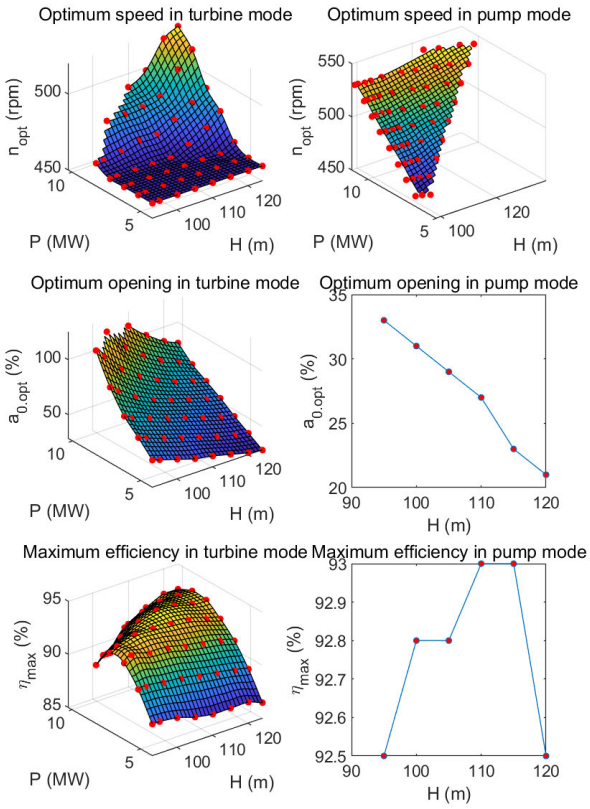

FIGURE 6. Optimization results of the variable-speed unit in two modes.

TABLE 1. Amplitude variation of the head.

Project	Power (MW)	$H_{p.max}$ (m)	$H_{p.max}$ (m)	$H_{p.max}$ (m)	Manufacturer
Yagisawa, Japan	85	112.5	53	2.12	Toshiba
Takami, Japan	100	115.2	80.6	1.43	Mitsubishi
Ohkawachi, Japan	395	432	342	1.26	Hitachi
Nant de Drance, Switzerland	157	395	250	1.58	Alstom
Linthal, Switzerland	250	724	560	1.29	GE
Tehri, India	250	227	127	1.79	Alstom

vibration, may occur at too high or too low speed. Appropriate speed operation ranges should be carefully considered.

In fact, the ranges should meet the objective conditions of the pumped storage plant and the actual requirements of the power grid, which means that it should adjust the sustainable change of the operating conditions. According to the current standard and engineering experience [38], [39], the maximum-minimum head ratio's limit value reaches from 1.25 to 1.45 for a fixed-speed unit. However, it can reach two or higher after adopting a variable-speed unit. The head's amplitude variation in some variable-speed pumped storage plants is shown [7], [40], [41] (see Table 1).

Rated optimum operating point (Q_{110}, n_{110}) is close to the center of the iso-efficiency circle, and we have

$$n_{110} = \frac{n_r D}{\sqrt{H_d}} \tag{17}$$

where n_r is the rated speed and H_d is the design head.

For variable-speed operation, speed is set to n. Mathematically,

$$n = \frac{n_{110}\sqrt{H}}{D} = \frac{n_r D}{\sqrt{H_d}}\frac{\sqrt{H}}{D} = n_r\sqrt{\frac{H}{H_d}} \tag{18}$$

Therefore, speed n is in proportion to $H^{0.5}$, and the difference with rated speed is Δn.

$$\Delta n = n_r\left(\sqrt{\frac{H}{H_d}} - 1\right) \tag{19}$$

When $H < H_d$, the speed is lower than the rated speed, and vice versa. According to the head variation data of the above-mentioned pumped storage stations, at the same time, the design head will be higher than the average head.

$$H_{max} - H_r < H_r - H_{min} \tag{20}$$

$$1.45 \le \frac{H_{max}}{H_{min}} \le 2 \tag{21}$$

where H_{min} and H_{max} is the limit value of head variation, H_r is the rated head of the variable-speed unit, and the head variation range is between 1.45 and 2.

If $H_{max}/H_r = a > 1$ and $H_{min}/H_r = b < 1$, a and b will drop into the blue zone in Fig.7.

Finally, we design $H_{max}/H_r = 1.25$ and $H_{min}/H_r = 0.65$, namely point S in Fig.7. The corresponding upper and lower bounds of the speed are $1.118n_r$ and $0.806n_r$, respectively. The amplitude of adjustment is 31.2%, with the corresponding variation range of the AC excitation frequency from −5.9 Hz to 9.7 Hz. The negative sign means the magnetic field's rotational direction is opposite to the direction of the shaft. The unit's speed range in the actual engineering also needs to consider the motor-generator and converter's technical and economic issues. From the above analysis, different heads correspond to different ranges of speed. Fig. 8 shows the unit speed variation with different heads in this case. The upper and lower bound of unit speed are $1.39n_{110}$ and $0.72n_{110}$, respectively. As the unit speed is limited to a small range, this will improve the steady-state model's regression effect.

B. OPTIMUM SPEED AND GATE OPENING MODEL AND ITS SIMPLIFICATION

1) OPTIMUM SPEED MODEL AND ERROR ANALYSIS

The complexity of a model depends on its purpose [42], [43]. There are many non-linear and high order models in the dynamic system used for control design, which cannot adapt to the steady-state studies on a large time scale due to their long operation time and large resource consumption. However, the steady-state model used for planning and scheduling mainly focuses on power optimization and energy distribution in time and space, rather than the transient transition process. Therefore, it is urgent to propose reduced-order models.

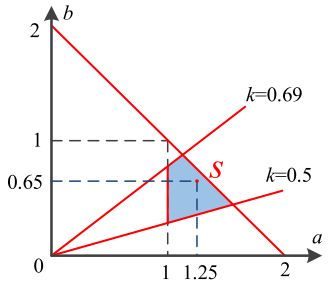

FIGURE 7. Head ranges of the variable-speed pumped storage plant.

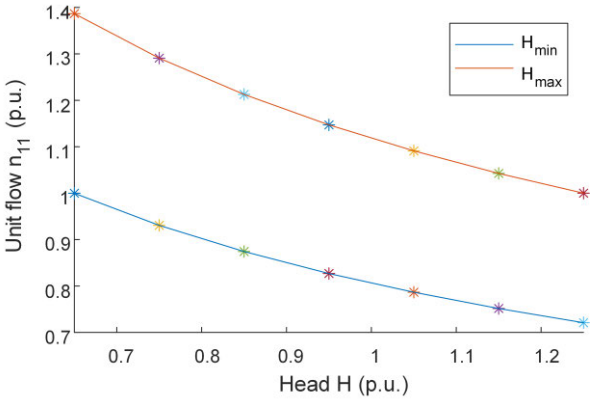

FIGURE 8. Unit speed variation with different heads.

First, the iso-efficiency circle of the Hill Chart is further investigated. It can be found that the optimum operating condition curve $C3$: $n_{11} \sim Q_{11.\mathrm{opt}}$ is monotonically increasing in most cases and is approximately linear near the rated operating condition. The correlation coefficient is r_1.

In addition, based on $P_{11.\max} = 9.81 Q_{11.\mathrm{opt}} \eta_{\max}$, the change of the maximum efficiency $\Delta\eta_{\max}$ is far less than that of the unit flow $\Delta Q_{11.\mathrm{opt}}$ in curve $C3$. Therefore, it can also be considered that there is an approximate strong linear relationship between $P_{11.\max}$ and $Q_{11.\mathrm{opt}}$. The correlation coefficient is $r_2 \to 1$.

Based on the above two aspects, it can be concluded that there is an approximately linear relationship between $P_{11.\max}$ and $n_{11.\mathrm{opt}}$ near the rated operating condition as follows:

$$P_{11.max} \approx a n_{11.opt} + b \tag{22}$$

where a and b are constant coefficients. Moreover, the correlation coefficient is r_3.

Since $r_2 \to 1$, it can be considered that r_1 is the main factor affecting the degree of linear correlation between $P_{11.\max}$ and $n_{11.\mathrm{opt}}$, that is, $r_3 \approx r_1$. The proof is given below.

PROOF: Without losing generality, subtracting constant or dividing constant does not change the correlation coefficient between variables. Assume that A, B, and X are all random variables with a mean value of zero and a standard deviation of 1.

Through linear regression, A and B are each decomposed into two parts, one is wholly related to X, and the other is completely unrelated to X:

$$A = \rho_A X + \epsilon_A \tag{23}$$

$$B = \rho_B X + \epsilon_B \tag{24}$$

where the mean value of ϵ_{A} and ϵ_{B} is zero and is not related to the random variable X. Calculate the variance on both sides of the equation, with

$$Var\left(\epsilon_A\right) = 1 - \rho_A^2 \sigma_X^2 = 1 - \rho_A^2 \tag{25}$$

$$Var\left(\epsilon_B\right) = 1 - \rho_B^2 \sigma_X^2 = 1 - \rho_B^2 \tag{26}$$

Calculate the correlation coefficient between A and B.

$$\begin{aligned} Corr(A,B) &= \frac{Cov(A,B)}{\sqrt{Var(A)Var(B)}} \\ &= Cov\left(\rho_A X + \epsilon_A, \rho_B X + \epsilon_B\right) \\ &= \rho_A \rho_B Var(X) + Cov\left(\epsilon_A, \epsilon_B\right) \\ &= \rho_A \rho_B + Corr\left(\epsilon_A + \epsilon_B\right) Std\left(\epsilon_A\right) Std\left(\epsilon_B\right) \\ &= \rho_A \rho_B + Corr\left(\epsilon_A + \epsilon_B\right) \sqrt{1-\rho_A^2}\sqrt{1-\rho_B^2} \end{aligned} \tag{27}$$

It can be seen from (27) that when ρ_{A} and ρ_{B} are given, $Corr(A, B)$ is only determined by $Corr(\epsilon_{\mathrm{A}}, \epsilon_{\mathrm{B}})$.

When $\rho_{\mathrm{A}} \to 1$, we have

$$Corr(A,B) \approx Corr(B) = \rho_B \tag{28}$$

So, when $r_2 = Corr(P_{11.\max}, Q_{11.\mathrm{opt}}) \to 1$, we have

$$r_3 = Corr\left(P_{11.max}, n_{11.opt}\right) \approx Corr\left(Q_{11.opt}, n_{11.opt}\right) = r_1 \tag{29}$$

Proof completed.

Substituting (1) and (22) into (3), we have

$$P \approx \left(a n_{11.opt} + b\right) D^2 H \sqrt{H} = a D^3 n_{opt} H + b D^2 H \sqrt{H} \tag{30}$$

1) When diameter D and head H are constants, we have

$$P \approx a D^3 H \cdot n_{\mathrm{opt}} + b D^2 H \sqrt{H} = k_1 n_{\mathrm{opt}} + k_2 \tag{31}$$

where k_1 and k_2 are constant coefficients.

2) When D and n_{opt} are constants, $H^{1.5}$ is expanded by Taylor series at rated head H_{r}. So we have

$$H\sqrt{H} = H_r\sqrt{H_r} + 1.5\sqrt{H_r}\left(H - H_r\right) + o\left[\left(H - H_r\right)\right] \tag{32}$$

where $|H - H_r| < |H_r|$.

The Lagrange Error Bound of (32) is analyzed as follows. First,

$$\begin{aligned} o\left[\left(H-H_r\right)^2\right] &= R_n(x) \\ &\le \left| \max_{\substack{a \le c \le x \\ or\ x \le c \le a}} \frac{f^{n+1}(c)}{(n+1)!}(x-a)^{n+1} \right| \end{aligned} \tag{33}$$

where c is a value between x and a.

Substituting $f(H) = H^{1.5}$ and $n = 1$ into (33), we have

$$\begin{aligned} & o\left[(H - H_r)^2\right] \\ & \leq \left| \begin{array}{c} max \\ H_r \leq h \leq H \\ or\ H \leq h \leq H_r \end{array} \frac{\left(H\sqrt{H}\right)''\Big|_{H=h}}{2} (H - H_r)^2 \right| \\ & = \left| \begin{array}{c} max \\ H_r \leq h \leq H \\ or\ H \leq h \leq H_r \end{array} \frac{3}{8\sqrt{h}} (H - H_r)^2 \right| \end{aligned} \tag{34}$$

From the analysis of Part A in Section IV, we have obtained $H_{\max}/H_{\mathrm{r}} = 1.25$ and $H_{\min}/H_{\mathrm{r}} = 0.65$. Then, when $h = H = H_{\min}$, the right side's maximum value in (34) can be obtained. So far, we have

$$o\left[(H - H_r)^2\right] \leq 0.057 H_r \sqrt{H_r} \tag{35}$$

The maximum percentage error relative to the design head H_{r} is

$$Max.Pct.Error = \frac{0.057 H_r \sqrt{H_r}}{H\sqrt{H}}\Big|_{H=H_r} = 5.7\% \tag{36}$$

So far, it can be shown that in the typical scenario in this paper, the error of Lagrange remainder in (32) is small and will not exceed the error range of engineering application. Thus, substituting (32) into (30) is completely valid.

$$\begin{aligned} P &\approx \left(aD^3 n_{opt} + 1.5bD^2\sqrt{H_r}\right) \cdot H - 0.5bD^2 H_r \sqrt{H_r} \\ &= k_3 H + k_4 \end{aligned} \tag{37}$$

where k_3 and k_4 are constant coefficients.

To sum up, there is an approximately linear relationship between the output power P and the head H and optimum speed n_{opt} near the rated operating condition, so we set the optimum speed-head-power characteristic model as follows:

$$n_{\mathrm{opt}} = b_1 P + b_2 H + b_3 \tag{38}$$

where b_1, b_2, and b_3 are constant coefficients.

Based on the above analysis, we can see that the model's error mainly comes from two parts: the linearization degree ($r_1 = Corr(n_{11.\mathrm{opt}}, Q_{11.\mathrm{opt}})$) of the optimum operating condition curve $C3$ and the linearization error caused by Taylor expansion at the design head H_{r}.

The unit speed does not need to be taken over the entire Hill Chart, and this will cause a significant error. Fortunately, as mentioned earlier, the unit speed range is ($0.72n_{110}$, $1.39n_{110}$). The optimum unit speed will avoid operating conditions where the unit flow is too small or too large. These operating conditions are precisely the "bad points" that make the linear regression degree of the optimal operating curve condition worse. Besides, the 95% output limit line restriction can further prevent the unit from entering the highly nonlinear and unstable operation area, which is beneficial to improve the linear regression degree of the model.

2) OPTIMUM GATE OPENING MODEL AND ERROR ANALYSIS

In terms of gate opening optimization, the optimum operating condition curve $C3$: $Q_{11.\mathrm{opt}} \sim n_{11.\mathrm{opt}}$ intersects each iso-opening curve in the Hill Chart. The curve of intersection points is the optimum gate opening curve $C5$: $Q_{11.\mathrm{opt}} \sim a_{0.\mathrm{opt}}$. Obviously, the distribution of the iso-opening curve shows that the optimum opening curve $C5$ is better linearized than the curve $C3$. There is an approximately linear relationship between $P_{11.\max}$ and $Q_{11.\mathrm{opt}}$, then

(1) When D and H are constants, $P = P_{11.\max} D^2 H^{1.5} \propto P_{11.\max}$. Therefore, there is an approximately linear relationship among P, $Q_{11.\mathrm{opt}}$, and $a_{0.\mathrm{opt}}$.

(2) When D and $a_{0.\mathrm{opt}}$ are constants, $Q_{11.\mathrm{opt}}$, and $P_{11.\max}$ are also uniquely determined. According to the formula $P = P_{11.\max} D^2 H^{1.5} \propto H^{1.5}$ and the Taylor formula, it has the same approximate linear relationship between P and H.

Finally, an optimum opening-head-power characteristic model is proposed as follows:

$$a_{0.\mathrm{opt}} = b_4 P + b_5 H + b_6 \tag{39}$$

where b_4, b_5, and b_6 are constant coefficients.

Unlike modeling methods such as look-up table, higher-order regression, and some artificial intelligence approaches, the linear model dramatically simplifies the variable-speed unit's optimum characteristic within its specific scope of application.

V. MODEL VALIDATION

In this section, simulation analysis is conducted based on different turbines with different specific speeds for model validation and error analysis.

Section IV analyzes the error influencing factors, namely, 1) the linearization degree of optimum operating condition curve $C3$, and 2) the linearization error caused by Taylor expansion at the design head H_{r}. Model validation is tested in multiple scenarios in this section. The usage scenarios and matters needing attention of the optimum speed and gate opening models are studied by comparing models of different types and with different specific speeds. The Hill Chart is the original data (refer to Appendix), and the $H{\sim}P$ operation curve is the validation data. The results are shown in Table 2.

It can be seen from Table 2, for the runners with different specific speeds, the optimal speed linear model can well track the optimal operating condition, and the R_2 is generally greater than 0.95 or even 0.99, indicating that the linear regression degree is high. The p-value is very low, indicating that the fitting reliability is high. Comparing the fitting degree between the linear model and curve $C3$ as shown in Fig. 9, it can be found that, in general, the R^2 of the two curves have the same trend with the Pearson coefficient is 0.7396, which shows the significant correlation (0.5∼0.8). As shown from the above results, the results largely depend on the linearity and slope of the optimum operating condition curve $C3$: $n_{11.\mathrm{opt}} \sim Q_{11.\mathrm{opt}}$. The shape of the Hill Chart of the turbine can affect the precision of models to the maximum extent. Besides, considering the constant-coefficient b_1, b_2 and b_3,

TABLE 2. Predictive value from optimum models with different runners.

No.	Cases	Specific speed n_s	H (m)	P (10^3 kW)	Linear model for optimal speed ($n_{opt}=b_1P+b_2H+b_3$)			Linear regression of the curve $n_{11.opt}$~$Q_{11.opt}$	
					Coefficient (b_1,b_2,b_3)	R^2	p-value	Slope	R^2
1	Fig.5 in [44]	189	[100,150]	[22,52]	0.0041, -0.1320, 238.0177	**0.97985**	1.16E-06	16.1989	**0.60381**
2	Fig.4(a) in [19]	211	[45,70]	[5,23]	0.0024, 1.2255, 146.6256	**0.96157**	4.28E-07	7.5489	**0.79882**
3	Fig.5 in [45]	238	[45,70]	[6,23]	-0.0001, 2.0994, 143.505	**0.81899**	2.52E-03	11.5288	**0.41006**
4	Fig.2 in [46]	101	[90,140]	[5.5,10.5]	0.0228, -0.4955, 299.9599	**0.99269**	3.33E-08	126.8659	**0.94709**
5	Fig.2(a) in [47]	225	[100,150]	[22,52]	-0.0013, 2.0791, 175.8707	**0.98162**	8.42E-07	29.514	**0.82509**
6	Fig.2(b) in [47]	162	[110.140]	[12,30]	0.0046, -0.2409, 293.6183	**0.86431**	0.00092035	22.3203	**0.54452**
7	Fig.2(c) in [47]	131	[150,225]	[11,30]	-0.0023, 1.4883, 176.4362	**0.99776**	0.59141	25.8084	**0.59141**
8	Fig.2(d) in [47]	81	[175,225]	[11,28]	0, 1.0163, 216.9142	**0.99096**	7.04E-08	15.8774	**0.81743**

The diameter D of the runner is 5 m.

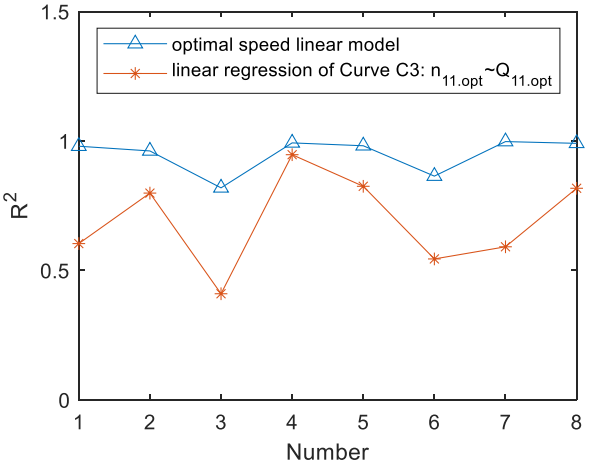

FIGURE 9. Comparison of R^2 trends.

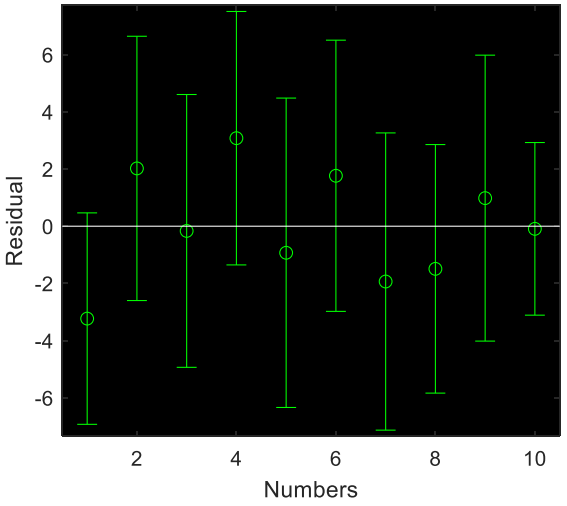

FIGURE 10. Residual graph of sampling points.

the weight of output P is lower, and the weight of intercept b_3 is higher based on the SI system (kW, m, rpm).

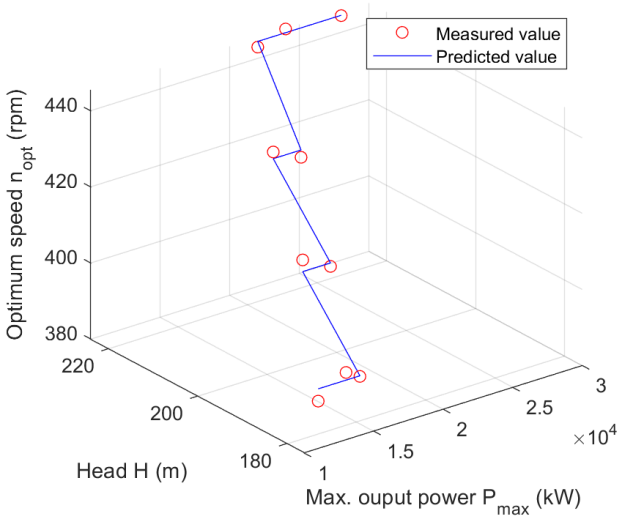

FIGURE 11. Comparison between measured and predicted values.

Taking case 8 as the example, we can get the residual graph of sampling points (see Fig.10), the comparison between measured values and fitted values (see Fig.11), and the percentage error graph (see Fig.12). It can be found that there are no abnormal points in the residual graph, and the error of each point is less than 1%.

Also, take Case 8 as an example; we have verified the error accumulation caused by the operating head H deviation from the design head H_r. Moreover, observe the prediction error of the model through the different heads. The results are shown in Fig. 13 and Fig. 14.

In this scenario, the rated design head H_r is 250 m, the minimum and maximum heads are 150 m and 300 m. $H_{max}/H_{min} = 2$. As can be seen from Fig.13 and Fig.14, when the power is constant (15 MW) near the design head H_r (250 m), the absolute percentage error between the actual value and the predicted value obtained by the optimal speed

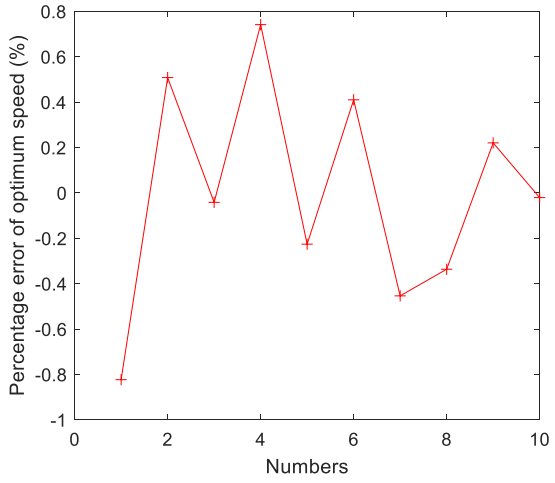

FIGURE 12. Percentage error between measured and predicted values.

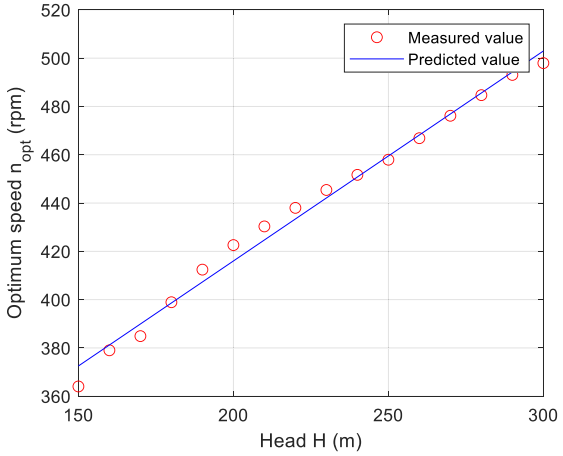

FIGURE 13. Comparison of optimum speed at the different head (P = 15 MW).

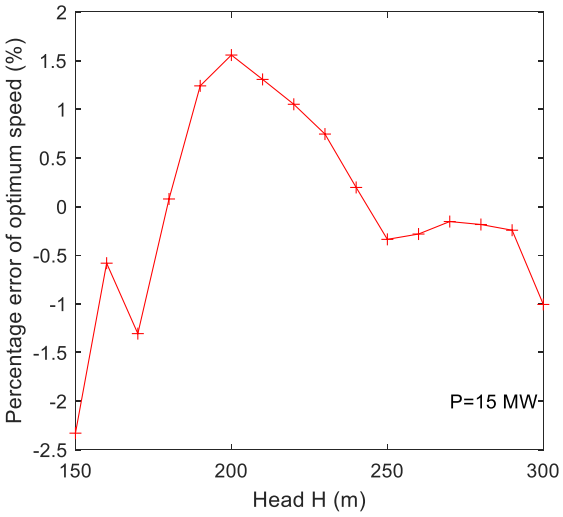

FIGURE 14. Percentage error of optimum speed at the different head (P = 15 MW).

linear model is the smallest, less than 0.5%. When the operating head deviates far from the design head H_r, the absolute error gradually increases. When the head reaches 150 m, the absolute percentage error reaches 2.33%. The greater the head's deviation, the greater the model's error. It is determined by the Lagrange Error Bound in the model simplification process and cannot theoretically be eliminated. Fortunately, in a variable-speed unit's typical operating scenario, the operating head generally does not deviate too much from the design head. Even if H_{max}/H_{min} reaches two (this is not a common phenomenon), the absolute error is less than 5%, completely acceptable in engineering.

The same process method can be used to verify the optimum gate opening linear model, which will not be repeated in this paper.

VI. CONCLUSION AND FUTURE WORK

Based on the performance curves of a model pump and the Hill Chart of a model turbine, an optimization method for variable-speed pumped storage units in two modes is proposed, with the goal of efficiency optimization in turbine mode and power tracking in pump mode. Secondly, the concept of "Steady operation area in non-optimum condition" of the variable-speed unit is proposed. Finally, a reduced-order steady-state model of the variable-speed unit is established. Based on the error analysis of several typical scenarios, the feasibility of the model is verified.

The conclusions are as follows:

1) In turbine mode, the Hill Chart based optimization method is proposed. The variable-speed unit can track the steady-state optimal operating conditions in real-time to achieve maximum efficiency.
2) In pump mode, the optimal speed and gate opening can be obtained through the performance curves without the Hill Chart. Extending the operating range of input power is the most exciting advantage in pump mode, not the efficiency gain.
3) Considering the influence of the optimal operating condition curve on the optimization strategy when it is not monotonous, the concept of "steady operation area in non-optimum condition" is proposed.
4) The optimal linear model dramatically simplifies the steady-state model of the variable-speed unit. Two main factors affect the accuracy of the model: the first is the shape of the Hill Chart, such as the degree of linearization and slope of the optimum operating curve; the second is the degree of deviation of the actual operating head from the design head. Verified by multiple scenarios, the absolute error is within 5%, completely acceptable in engineering.

Future work will focus on the simplified model of the variable-speed pumped storage unit in the hydraulic transition process. We hope to achieve the ideal simulation effect with the minimum consumption of computing resources to study the variable-speed unit's dynamic response after a large-scale grid connection.

APPENDIX

Appendixes contain all the optimal operating condition data from case 1 to case 8 to verify the optimal linear model. https://dx.doi.org/10.21227/jfay-qa71

REFERENCES

[1] X. Gong, F. Dong, M. A. Mohamed, E. M. Awwad, H. M. Abdullah, and Z. M. Ali, "Towards distributed based energy transaction in a clean smart island," *J. Cleaner Prod.*, vol. 273, Nov. 2020, Art. no. 122768.

[2] M. A. Mohamed, T. Jin, and W. Su, "An effective stochastic framework for smart coordinated operation of wind park and energy storage unit," *Appl. Energy*, vol. 272, Aug. 2020, Art. no. 115228.

[3] P. Donalek, "Role for adjustable speed pumped storage in the grid of the future," presented at the CIGRE Grid Future Symp., Cleveland, OH, USA, Oct. 2017.

[4] F. Geth, T. Brijs, J. Kathan, J. Driesen, and R. Belmans, "An overview of large-scale stationary electricity storage plants in europe: Current status and new developments," *Renew. Sustain. Energy Rev.*, vol. 52, pp. 1212–1227, Dec. 2015.

[5] R. Jiang, J. Wang, and Y. Guan, "Robust unit commitment with wind power and pumped storage hydro," *IEEE Trans. Power Syst.*, vol. 27, no. 2, pp. 800–810, May 2012.

[6] V. Koritarov, T. D. Veselka, J. Gasper, B. M. Bethke, A. Botterud, J. Wang, M. Mahalik, Z. Zhou, C. Milostan, J. Feltes, and Y. Kazachkov, "Modeling and analysis of value of advanced pumped storage hydropower in the United States," Argonne Nat. Lab., Lemont, IL, USA, Tech. Rep. ANL/DIS-14/7, Jun. 2014.

[7] K. R. Vasudevan, V. K. Ramachandaramurthy, G. Venugopal, J. B. Ekanayake, and S. K. Tiong, "Variable speed pumped hydro storage: A review of converters, controls and energy management strategies," *Renew. Sustain. Energy Rev.*, vol. 135, Jan. 2021, Art. no. 110156.

[8] M. Chazarra, J. I. Perez-Diaz, and J. Garcia-Gonzalez, "Optimal joint energy and secondary regulation reserve hourly scheduling of variable speed pumped storage hydropower plants," *IEEE Trans. Power Syst.*, vol. 33, no. 1, pp. 103–115, Jan. 2018.

[9] A. Joseph, K. Desingu, R. R. Semwal, T. R. Chelliah, and D. Khare, "Dynamic performance of pumping mode of 250 MW variable speed hydro-generating unit subjected to power and control circuit faults," *IEEE Trans. Energy Convers.*, vol. 33, no. 1, pp. 430–441, Mar. 2018.

[10] A. Joseph and T. R. Chelliah, "A review of power electronic converters for variable speed pumped storage plants: Configurations, operational challenges, and future scopes," *IEEE J. Emerg. Sel. Topics Power Electron.*, vol. 6, no. 1, pp. 103–119, Mar. 2018.

[11] E. D. Castronuovo and J. A. P. Lopes, "On the optimization of the daily operation of a wind-hydro power plant," *IEEE Trans. Power Syst.*, vol. 19, no. 3, pp. 1599–1606, Aug. 2004.

[12] J. A. Suul, K. Uhlen, and T. Undeland, "Wind power integration in isolated grids enabled by variable speed pumped storage hydropower plant," in *Proc. IEEE Int. Conf. Sustain. Energy Technol.*, Singapore, 2008, pp. 399–404.

[13] J. Schmidt, W. Kemmetmüller, and A. Kugi, "Modeling and static optimization of a variable speed pumped storage power plant," *Renew. Energy*, vol. 111, pp. 38–51, Oct. 2017.

[14] M. A. Bidgoli, W. Yang, and A. Ahmadian, "DFIM versus synchronous machine for variable speed pumped storage hydropower plants: A comparative evaluation of technical performance," *Renew. Energy*, vol. 159, pp. 72–86, Oct. 2020.

[15] M. Mohanpurkar, A. Ouroua, R. Hovsapian, Y. Luo, M. Singh, E. Muljadi, V. Gevorgian, and P. Donalek, "Real-time co-simulation of adjustable-speed pumped storage hydro for transient stability analysis," *Electr. Power Syst. Res.*, vol. 154, pp. 276–286, Jan. 2018.

[16] M. Chazarra, J. I. Perez-Diaz, and J. Garcia-Gonzalez, "Optimal operation of variable speed pumped storage hydropower plants participating in secondary regulation reserve markets," in *Proc. 11th Int. Conf. Eur. Energy Market (EEM)*, Market, Krakow, May 2014, pp. 1–5.

[17] J. L. Márquez, M. G. Molina, and J. M. Pacas, "Dynamic modeling, simulation and control design of an advanced micro-hydro power plant for distributed generation applications," *Int. J. Hydrogen Energy*, vol. 35, no. 11, pp. 5772–5777, Jun. 2010.

[18] A. Bostan, N. Dorian, and F. Peris-Bendu, "The hill chart calculation for francis runner models using the HydroHillChart-francis module software," *Analele Universitatii*, vol. 22, no. 1, pp. 107–116, 2015.

[19] I. Iliev, C. Trivedi, and O. G. Dahlhaug, "Variable-speed operation of francis turbines: A review of the perspectives and challenges," *Renew. Sustain. Energy Rev.*, vol. 103, pp. 109–121, Apr. 2019.

[20] H. Iman-Eini, D. Frey, S. Bacha, C. Boudinet, and J.-L. Schanen, "Evaluation of loss effect on optimum operation of variable speed micro-hydropower energy conversion systems," *Renew. Energy*, vol. 131, pp. 1022–1034, Feb. 2019.

[21] J. Fraile-Ardanuy, J. R. Wilhelmi, J. J. Fraile-Mora, and J. I. Perez, "Variable-speed hydro generation: Operational aspects and control," *IEEE Trans. Energy Convers.*, vol. 21, no. 2, pp. 569–574, Jun. 2006.

[22] K. Desingu, R. Selvaraj, T. R. Chelliah, and D. Khare, "Effective utilization of parallel-connected megawatt three-level back-to-back power converters in variable speed pumped storage units," *IEEE Trans. Ind. Appl.*, vol. 55, no. 6, pp. 6414–6426, Nov. 2019.

[23] T. Harbort, G. Lein, and E. Goede, "Power frequency control of a pump turbine as an example for the operation with adjustable speed of hydraulic machines," *IFAC Proc. Volumes*, vol. 30, no. 17, pp. 335–341, Aug. 1997.

[24] L. M. O. de Mesquita, J. dos Santos Menas, E. L. van Emmenk, and M. Aredes, "Maximum power point tracking applied on small hydroelectric power plants," in *Proc. Int. Conf. Electr. Mach. Syst.*, Beijing, China, Aug. 2011, pp. 1–6.

[25] J. I. Pérez, J. R. Wilhelmi, and L. Maroto, "Adjustable speed operation of a hydropower plant associated to an irrigation reservoir," *Energy Convers. Manage.*, vol. 49, no. 11, pp. 2973–2978, Nov. 2008.

[26] A. Borghetti, M. Di Silvestro, G. Naldi, M. Paolone, and M. Alberti, "Maximum efficiency point tracking for adjustable-speed small hydro power plant," in *Proc. 16th PSCC*, Glasgow, U.K., 2008, pp. 1–7.

[27] Z. Jiang, "Power conversion system for grid connected micro hydro power system with maximum power point tracking," M.S. thesis, Univ. Wisconsin Milwaukee, Milwaukee, WI, USA, USA, 2017.

[28] B. Guo, A. Mohamed, S. Bacha, and M. Alamir, "Variable speed micro-hydro power plant: Modelling, losses analysis, and experiment validation," in *Proc. 9th IEEE Int. Conf. Ind. Technol. (ICIT)*, Lyon, France, Feb. 2018.

[29] E. H. Sundfør, "Design and operation of a francis turbine with variable speed capabilities," M.S. Diss., Dept. Energy Process Eng., Norwegian Univ. Sci. Technol., Høgskoleringen, Norway, Jun. 2017.

[30] I. Iliev, E. O. Tengs, C. Trivedi, and O. G. Dahlhaug, "Optimization of Francis turbines for variable speed operation using surrogate modeling approach," *J. Fluids Eng.*, vol. 142, no. 10, Oct. 2020, Art. no. 101214.

[31] A. Morabito, G. de Oliveira e Silva, and P. Hendrick, "Deriaz pump-turbine for pumped hydro energy storage and micro applications," *J. Energy Storage*, vol. 24, Aug. 2019, Art. no. 100788.

[32] D. Schafer and J.-J. Simond, "Adjustable speed asynchronous machine in hydro power plants and its advantages for the electric grid stability," presented at the CIGRE, 1998. [Online]. Available: https://infoscience.epfl.ch/record/134078?ln=en

[33] W. Yao, C. Deng, D. Li, M. Chen, P. Peng, and A. H. Zhang, "Optimal sizing of seawater pumped storage plant with variable-speed units considering offshore wind power accommodation," *Sustainability*, vol. 11, no. 7, p. 1939, Apr. 2019.

[34] S. I. Abubakirov, M. E. Lunatsi, T. V. Plotnikova, P. V. Sokur, P. Y. Tuzov, V. N. Shavarin, Y. G. Shakaryan, and V. A. Shchur, "Performance optimization of hydraulic turbine by use of variable rotating speed," *Power Technol. Eng.*, vol. 47, no. 2, pp. 102–107, Jul. 2013.

[35] J. Delgado, L. Andolfatto, D. I. C. Covas, and F. Avellan, "Hill chart modelling using the Hermite polynomial chaos expansion for the performance prediction of pumps running as turbines," *Energy Convers. Manage.*, vol. 187, pp. 578–592, May 2019.

[36] *Hydraulic Turbines, Storage Pumps and Pump-Turbines—Model Acceptance Tests*, IEC Standard 60193, 2019.

[37] A. R. Simpson and A. Marchi, "Evaluating the approximation of the affinity laws and improving the efficiency estimate for variable speed pumps," *J. Hydraulic Eng.*, vol. 139, no. 12, pp. 1314–1317, Dec. 2013.

[38] *Design Guide for Pumped Storage Power Station*, (in Chinese), China Industry Standard DL/T5208-2005, 2005.

[39] M. Valavi and A. Nysveen, "Variable-speed operation of hydropower plants: A look at the past, present, and future," *IEEE Ind. Appl. Mag.*, vol. 24, no. 5, pp. 18–27, Sep. 2018.

[40] T. Wang, Z. Zhang, J. Zhao, and C. Wang, "Impact analysis of variable speed units on the layout of pumped-storage power station in China," (in Chinese), *Water Power*, vol. 44, no. 4, pp. 60–63, Apr. 2018.
[41] A. Iwadachi, K. Tani, and K. Aguro, "The design of adjustable-speed pump-turbine modified from existing constant-speed on Okutataragi Power Station," in *Proc. 19th Int. Conf. Elect. Mach. Syst.*, Chiba, Japan, Nov. 2016, pp. 13–16.
[42] M. A. Mohamed, T. Jin, and W. Su, "Multi-agent energy management of smart islands using primal-dual method of multipliers," *Energy*, vol. 208, Oct. 2020, Art. no. 118306.
[43] L. Belhadji, S. Bacha, I. Munteanu, A. Rumeau, and D. Roye, "Adaptive MPPT applied to variable-speed microhydropower plant," *IEEE Trans. Energy Convers.*, vol. 28, no. 1, pp. 34–43, Mar. 2013.
[44] X. Yang, C. Yang, C. Yue, D. Yao, and C. Yuan, "Optimized operation of hydropower plant with VSC HVDC unit connection," presented at the CIGRE AORC Tech. Meeting, Tokyo, Japan, May 2014.
[45] D. Vukosavic, D. Divac, Z. Stojanović, B. Stojanović, and D. Vučković, "Several hydropower production management algorithms," *J. Serbian Soc. Comput. Mech.*, vol. 3, no. 1, pp. 182–209, 2009.
[46] W. Cai, Y. Wang, H. Shi, M. Zhang, and Q. Xu, "Study on optimization strategy of speed and opening of variable speed pumped storage unit," (in Chinese), *Large Electr. Mach. Hydraulic Turbine*, vol. 271, no. 4, pp. 58–63, 2020.
[47] P. Guo, Z. Wang, L. Sun, and X. Luo, "Characteristic analysis of the efficiency hill chart of Francis turbine for different water heads," *Adv. Mech. Eng.*, vol. 9, no. 2, pp. 1–8, Jan. 2017.

WEIWEI YAO (Member, IEEE) received the B.S. and M.S. degrees in electrical engineering from China Three Gorges University, China, in 2010 and 2014, respectively. He is currently pursuing the Ph.D. degree with Wuhan University, China. His research interests include microgrids operation and seawater pumped storage system operation.

CHANGHONG DENG (Member, IEEE) received the Ph.D. degree from the School of Electrical Engineering, Wuhan University, Wuhan, China, in 2007. She is currently a Professor with Wuhan University. Her research interests include power system security and stability analysis, optimal control theory, and renewable energy integration.

PENG PENG received the B.S. and M.S. degrees in electrical engineering from the Huazhong University of Science and Technology, China, in 2010 and 2013, respectively. He is currently a Professional Engineer with China Southern Power Grid Power Generation Company. His research interest includes the operation and the management of pumped storage stations.